# Supplementary Information for "Summertime increases in upper ocean stratification and mixed layer depth" by Sallée and co-authors.

## Mixed layer depth change in the Southern Ocean

In this Supplementary Information section, we discuss the influence of the Southern Ocean in determining the global-mean mixed layer depth change, and the limitations of our conclusions in the Southern Ocean due to historical data sparsity.

While the largest trends in mixed layer depth are found in the Southern Ocean (see Figure 3c), this region has also traditionally been one of the most poorly sampled (Extended Data Figure 2a). The Southern Ocean-wide time series of mixed layer depth (Figure 5g) contains some large annual anomalies, so that it is conceivable that the trend resulting from this basin-scale time series could be primarily shaped by a few anomalous years. Further, our mapped trend results (Figure 3c) exhibit several regional dipoles of positive/negative trends in the Southern Ocean which might arise from data limitations. We here provide additional analysis to document how historical data scarcity in the Southern Ocean may affect the conclusions of our work.

**Impact of Southern Ocean changes on global-mean diagnostics.** Figure 3c shows that the largest mixed layer depth trends are found in the Southern Ocean. While this is also the region where the climatological mean mixed layers are the deepest, the Southern Ocean (30°S-90°S) is associated with a mean percentage change markedly larger than the global average: -4.3±1.6 % dec$^{-1}$ for the Southern Ocean mean versus -2.9±0.5 % dec$^{-1}$ for the global mean (Table S1). In comparison, the rest of the ocean (i.e., the global mean without the Southern Ocean: 90°N-30°S) is associated with a slightly lower mean percentage change than the global average: -2.3±0.1 % dec$^{-1}$ (Table S1). However, it is important to note that, despite the Southern Ocean's influence, the rest of the ocean is associated with a mixed layer depth change that is consistent with the global mean value.

**Sensitivity of the Southern Ocean-wide percentage change.** As discussed in the main document and illustrated by Figure 5, an alternative way to compute basin-scale mean percentage change is by producing time series of percentage anomaly (i.e., anomaly from the local seasonal cycle). In Figure 5g, we show such time series for the Southern Ocean circumpolar band of relatively deep summer mixed layer (the region associated with climatological mean mixed layer depths of $\sim$ 50–100 m). This alternative approach produces a mean percentage trend of -3.4±1.5% dec$^{-1}$ (red line in Figure S1), which is consistent with our gridded trends of -4.3±1.6 % dec$^{-1}$ for the Southern Ocean (Table S1). The two estimates differ slightly because the two methodologies are drastically different (one is based from a local regression analysis, while the other is based on basin-wide approach), and because the regions of interest are not identical; however, the two estimates are consistent within standard error envelopes.

The Southern Ocean-wide time series (Figure S1a) is associated with relatively large intraseasonal variability, as shown by the 33-66 percentile range. To explore the influence of this variability, we perform a first Monte Carlo experiment in which we repeat the trend calculation 1000 times but add, for each repetition of the calculation, random noise on the annual estimates that spans the 33-66 percentile ranges. The standard deviation around the trend is indicated by the red shading in Figure S1. The standard deviation of the 1000 experiments is 1.5 % dec$^{-1}$, showing that the uncertainty associated with intraseasonal

variability has a limited impact on the trend calculation (-3.4 $dec^{-1}$). The time series also exhibits some level of interannual variability (Figure S1a). To gauge the sensitivity of our trend calculation to interannual outliers, we now conduct a second Monte Carlo experiment in which we repeat the trend calculation 1000 times, but randomly subsampling 35 years (i.e., a jackknife resampling of 70% of the 1970-2018 range). The resulting trends are shown as a probability density function (PDF) computed from the 1000 experiments (Figure S1b). This exercise shows some sensitivity to the choice of year, but associated with a standard deviation of only 1.7 % $dec^{-1}$. Thus, the sensitivity of our results to a specific choice of year is only half of the estimated mean.

**Data limitation on local / regional scales in the Southern Ocean.** The preceding analysis provides confidence in the Southern Ocean-wide percentage mixed layer depth change, and quantifies the sensitivity of this change to intraseasonal and interannual variability. However, sensitivity can be larger on more local scales. In particular, our gridded trends display some dipoles of negative/positive trends in the Southern Ocean that require further investigation. We note that some of these dipoles align with the mean geostrophic circulation. Figure S2 shows the gridded trend (same as in Figure 3c), but with the mean dynamic topography from Aviso superimposed (https://www.aviso.altimetry.fr/en/data/products/auxiliary-products/mdt.html). The jets of the Antarctic Circumpolar Current (latitude band 40-60°S) are clearly visible, and the organisation of some of the dipoles along this mean circulation suggests that they could result from distinct dynamical regimes between the northern and southern flanks of a jet.

However, not all the dipole patches align with the mean circulation, so here we aim to dig deeper and document the individual observations at the locations of these dipoles. We select individual observations in two paradigmatic dipoles: one in the southeastern Pacific Ocean, and another in the Indian Ocean basin. Then, we produce time series in these patches (Figure S3) in the same way as we do for the Southern Ocean-wide time series. For each of the positive/negative areas in the two regions, we compute a trend (red lines in Figure S3), and its sensitivity to intraseasonal and interannual variability from Monte Carlo experiments (respectively, red and blue shading around the trends in Figure S3). For the two deepening areas, we see that the trends are relatively well constrained by observations, with some level of sensitivity that does not challenge our conclusions (Figure S3c,e). In the Indian Ocean sector, the positive trend is only subtle (Figure S3d) and is less well constrained with historical observations than in the negative trend area (Figure S3e); nonetheless, the comparison of the two areas points to distinct dynamics, especially in the best-observed period of 2005-2018. In the Pacific Ocean sector, the positive trend (Figure S3b) is clearly not well constrained by historical observations, and so the trend there should be treated with caution. We note, however, that in the best-observed period of 2005-2018 there are clearly different regimes of shallowing/deepening trends that are consistent with the emergence of a dipole.

**Conclusion.** Data sparseness can be a limitation in computing local / regional trends in the Southern Ocean. The local structure of the gridded trend should therefore be treated with caution. We note, however, that in the few cases examined here, change in the best-observed period (2005-2018) is consistent with the long-term estimated change, so that localised dipoles could well be associated with distinct dynamical regimes. At any rate, we will need to wait for more observations to extract firmer conclusions on the detailed regional structure of mixed layer trends. Beyond potential limitations on local scales, our sensitivity experiments show that basin-scale diagnostics are robust to data sparseness. Finally, while the largest deepening trends are observed in the Southern Ocean, the mean change over the rest of the ocean is consistent with the global-mean estimate of a widespread deepening of mixed layers.

| MLD change (% dec$^{-1}$) | Choice 1 | Choice 2 | **Mean** |
|---|---|---|---|
| Global ($90°N-90°S$) | -2.6±0.1 | -3.2±0.9 | **-2.9±0.5** |
| Southern Ocean ($30°S-90°S$) | -3.7±0.2 | -4.9±2.9 | **-4.3±1.6** |
| Rest of the ocean ($90°N-30°S$) | -2.2±0.1 | -2.5±0.1 | **-2.3±0.1** |

**Table S1. Mean 1970-2018 percentage change in MLD**. Table showing the global mean percentage change and the associated standard errors of the mixed-layer depth (MLD), and corresponding mean for Southern Ocean only (30°S-90°S), and the rest of the ocean (90°N-30°S). Choice 1 refers to the solution where local regressions are computed with covariance between observations; choice 2 is with assumption of no covariances between observations. Local trend estimates at each grid point are divided by the local climatological mean value, and the global mean and standard error of the global mean are then computed. Standard error is computed by propagating the local standard error produced by the regression method (see Methods in the main text).

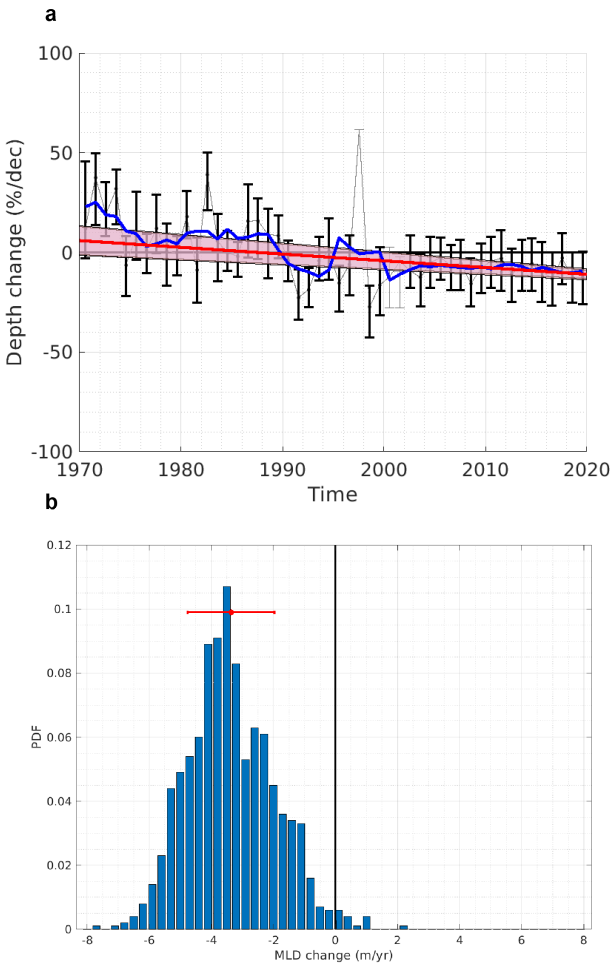


**Figure S1. Southern Ocean time series of mixed layer depth anomaly**. (a) Summer mixed layer depth anomaly times series and associated trend. Note that a negative depth anomaly refers to a deepening. Each times series panel shows: in thin gray line, the annual median percentage anomaly (from the local climatological seasonal cycle), computed for each individual observation; the errorbars refer to the 33-66 percentile range of percentage anomaly (errorbars are shown in black (gray) when more (fewer) than 50 data points are used in the annual statistics); the associated 5-year smoothed median time series is superimposed in blue; a linear trend from 1970-2018 is shown by the red line; the standard deviation of the Monte Carlo experiment exploring the sensitivity of the trend to the annual 33-66 percentile ranges is shown as red shading around the trend. (b) Probability density function (PDF) of linear trends resulting from the Monte Carlo experiment in which 35 years out of the 1970-2018 period are sub-sampled randomly, exploring the sensitivity of the trend calculation to a choice of specific set of years.

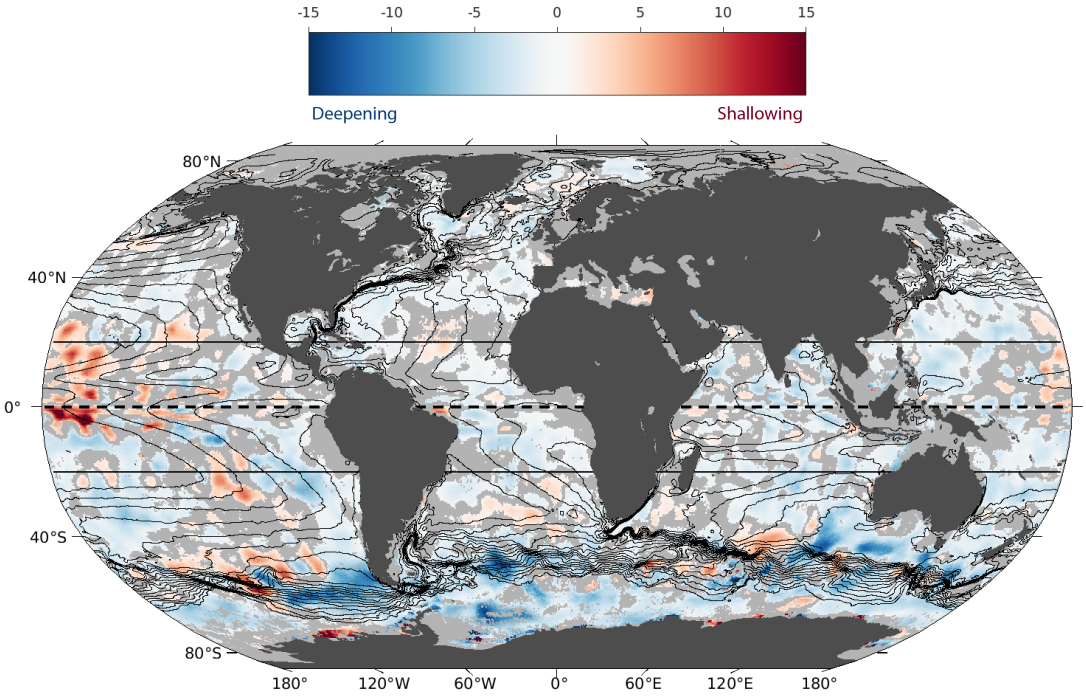


**Figure S2. 1970-2018 trends of mixed layer depth**. Map of the 1970-2018 summer mixed layer trend in m dec$^{-1}$ (same as in Figure 3c), but here the climatological mean dynamic topography is superimposed as black contours.

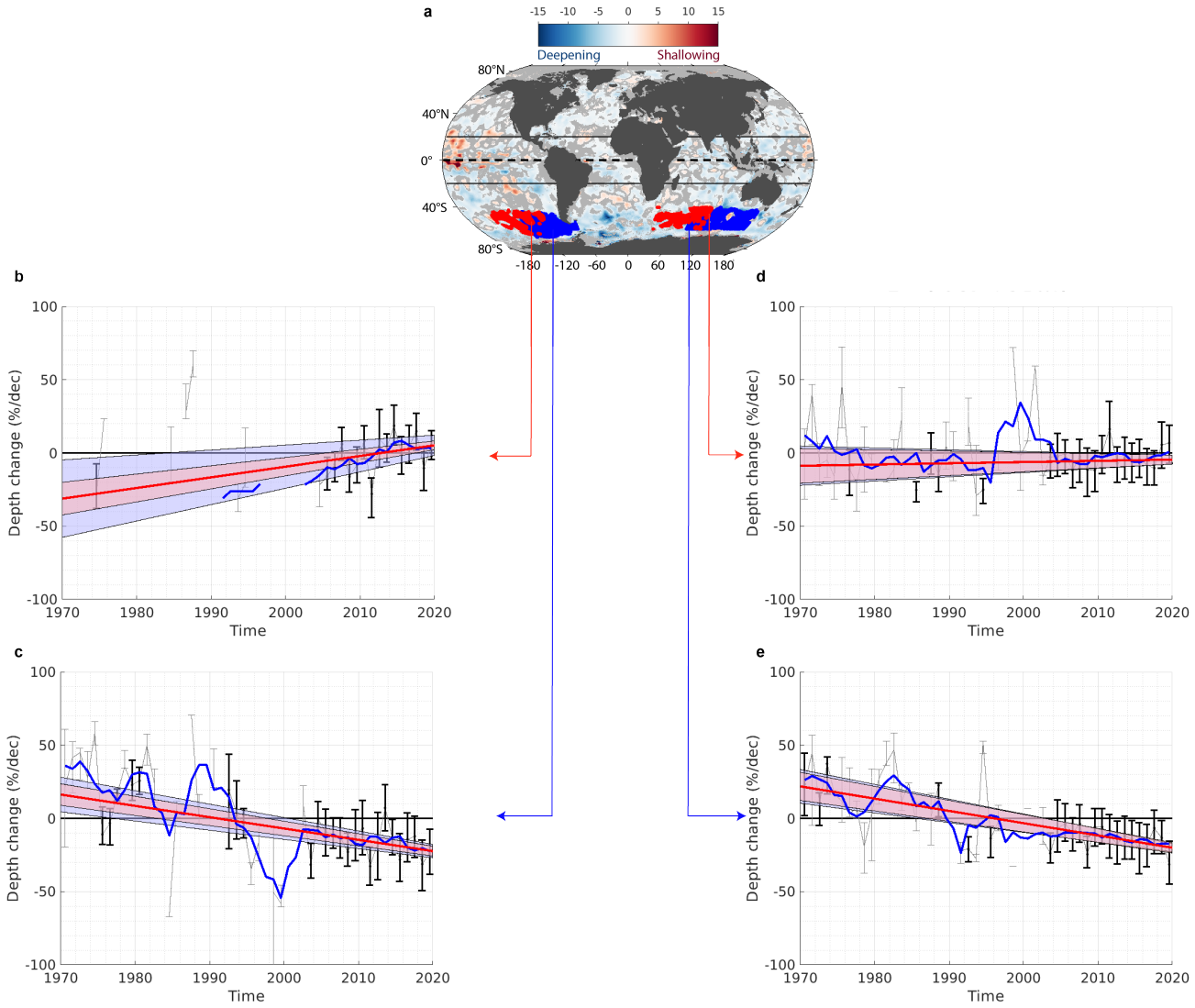


**Figure S3. Regional time series of mixed layer depth anomaly in the Southern Ocean negative/positive dipoles**. (a) Map of the 1970-2018 summer mixed layer trend in m $dec^{-1}$. Regional time series of mixed layer depth anomaly in the southeastern Pacific dipole is shown in panels (b,c) for the shallowing (b) and deepening (c) sectors. Regional time series of mixed layer depth anomaly in the south Indian dipole is shown in panels (d,e) for the shallowing (d) and deepening (e) sectors. The time series are constructed in the same way as in Figure S1, but with additional blue shading around the trend representing the standard deviation of the Monte Carlo experiment in which 70% of the number of available years are sub-sampled randomly, exploring the sensitivity of the trend calculation to a choice of specific set of years.